Front. Chem. Sci. Eng. 2023, 17(4): 460−469
https://doi.org/10.1007/s11705-022-2224-5

RESEARCH ARTICLE

Removal of nitric oxide from simulated flue gas using aqueous persulfate with activation of ferrous ethylenediaminetetraacetate in the rotating packed bed

Da Guo[1,2], Guisheng Qi (✉)[1,2], Dong Chen[1,2], Jiabao Niu[1,2], Youzhi Liu[1,2], Weizhou Jiao[1,2]

1 Shanxi Province Key Laboratory of Higee-Oriented Chemical Engineering, North University of China, Taiyuan 030051, China
2 School of Chemistry and Chemical Engineering, North University of China, Taiyuan 030051, China

Abstract Nitric oxide being a major gas pollutant has attracted much attention and various technologies have been developed to reduce NO emission to preserve the environment. Advanced persulfate oxidation technology is a workable and effective choice for wet flue gas denitrification due to its high efficiency and green advantages. However, NO absorption rate is limited and affected by mass transfer limitation of NO and aqueous persulfate in traditional reactors. In this study, a rotating packed bed (RPB) was employed as a gas–liquid absorption device to elevate the NO removal efficiency (η_{NO}) by aqueous persulfate ($(NH_4)_2S_2O_8$) activated by ferrous ethylenediaminetetraacetate (Fe^{2+}-EDTA). The experimental results regarding the NO absorption were obtained by investigating the effect of various operating parameters on the removal efficiency of NO in RPB. Increasing the concentration of $(NH_4)_2S_2O_8$ and liquid–gas ratio could promoted the oxidation and absorption of NO while the η_{NO} decreased with the increase of the gas flow and NO concentration. In addition, improving the high gravity factor increased the η_{NO} and the total volumetric mass transfer coefficient ($K_G\alpha$) which raise the η_{NO} up to more than 75% under the investigated system. These observations proved that the RPB can enhance the gas–liquid mass transfer process in NO absorption. The correlation formula between $K_G\alpha$ and the influencing factors was determined by regression calculation, which is used to guide the industrial scale-up application of the system in NO removal. The presence of O_2 also had a negative effect on the NO removal process and through electron spin resonance spectrometer detection and product analysis, it was revealed that Fe^{2+}-EDTA activated $(NH_4)_2S_2O_8$ to produce $\bullet SO_4^-$, $\bullet OH$ and $\bullet O_2^-$, played a leading role in the oxidation of NO, to produce NO_3^- as the final product. The obtained results demonstrated a good applicable potential of RPB/PS/Fe^{2+}-EDTA in the removal of NO from flue gases.

Keywords rotating packed bed, Fe^{2+}-EDTA, sulfate radical, hydroxyl radical, NO removal efficiency

1 Introduction

Nitrogen oxides (NO_x, NO ~90% or more, NO_2 ~10%) and SO_2 are the main pollutants, produced by burning coal in the iron, steel, coking, industrial kilns and boilers and cause adverse effect on environment (photochemical smog, acid rain and water eutrophication) and human health (respiratory system and cardiovascular disease) [1–3]. The state has promulgated the ultra-low emission standards of SO_2 and NO_x for steel and other enterprises, and are controlled at 35 and 50 $mg\cdot m^{-3}$ respectively [4]. The strict emission regulations require further development of coal-fired flue gas emission control technology. For the reduction of SO_2 and NO_x emission, the common technologies can be organized in two categories: the one is combustion control method and the other is post-combustion control method [5]. At present, wet flue gas desulfurization and selective catalytic reduction or selective non-catalytic reduction methods can effectively reduce SO_2 and NO_x emissions, but due to the huge system, the investment cost, large area, high operating temperature and secondary pollution [6,7], it is difficult to apply these methods to sintering plants and other small and medium-sized boilers. Wet scrubbing is recognized as a kind of promising flue gas purification technology due to its simple process [8]. Reduction, complex formation and oxidation are the three most common pathways for wet washing and simultaneous desulfurization and

Received May 27, 2022; accepted July 23, 2022

E-mail: zbdxqgs@126.com

denitrification process [9–12]. However, high costs or technical problems hinder the practical application of reduction and complex absorption technologies.

Oxidation absorption technologies are to oxidize insoluble NO into higher NO_x, which is the most widely studied denitrification process. Therefore, screening and developing the cost-effective oxidants to improve the solubility of NO in water is the key to oxidative denitrification process. Hence, the use of NaClO [13], $NaClO_2$ [14], $KMnO_4$ [15], H_2O_2 [16], peroxymonosulfate (PMS) [17] and persulfate (PS) [18], etc. for this purpose are the current research hotspots. In contrast, PS is a cost-effective and environmentally friendly oxidant with standard oxidation−reduction potential to be E_0 = +2.01 V, which shows its strong oxidizing properties. It is also more stable than H_2O_2 and is easy to store and transport. Some studies have shown that the $\bullet SO_4^-$ and •OH produced by PS activation bears high redox potential and strong oxidizing ability, hence high removal efficiency for the pollutants can be achieved [19,20]. At the same time, heat, ultraviolet radiation, ultrasound and transition metal ions can also effectively activate the $\bullet SO_4^-$ and •OH produced by PS [21]. The use of Fe^{2+} homogeneous activation of PS in the activation of transition metals has attracted wide attention [22,23], because of its low price, easy activation process, high efficiency, and no requirement for additional energy. However, Fe^{2+} is easy to inactivate and the large accumulation of Fe^{3+} in the system will cause the decreased reaction rate [24]. The chelating agent ethylenediaminetetraacetic acid (EDTA) is often added to form a complex with Fe^{2+} to adjust and maintain the concentration of Fe^{2+} to reduce unnecessary losses [25], while promoting Fe^{2+} regeneration and reducing Fe^{3+} accumulation. Adewuyi et al. [26] also showed that the removal efficiency of NO in the Fe^{2+}-EDTA system is much higher than that of achieved in the Fe^{2+} activation system, and revealed that Fe^{3+}-EDTA and Fe^{2+}-EDTA (NO) can be converted into Fe^{2+}-EDTA. Meanwhile, some studies [26–28] also showed that the gas–liquid mass transfer resistance during the oxidation of NO had a great influence on NO removal efficiency (η_{NO}) in traditional reactors such as bubbling towers. Liu et al. [29] designed an impinging stream reactor and investigated its removal performance for NO and SO_2 using PMS with synergic activation of Cu^{2+}/Fe^{3+} at high temperature, and found that the NO absorption rate was increased by increasing the gas phase mass transfer coefficient and interfacial area in the reactor structure. Chen and Hu [30] had developed a multi-stage bubble reactor combined with an agitator, which increased the NO content in liquid and promote the gas–liquid mass transfer. Thus, selecting a reactor with high mass transfer efficiency to enhance gas–liquid mass transfer is the key task to improve η_{NO} and reduce reactor volume during this research.

Rotating packed bed (RPB), as the main device of high gravity technology, can enhance the gas–liquid mass transfer process in a high centrifugal force field. In the RPB, when the fluid passes through the filler, the high-speed rotating filler generates strong shear force and converts it into droplets, liquid film and liquid mist, which greatly increase the interface and surface renewal rate of the transfer between phases [31]. This intensifies the mass transfer process and micro-mixing of the gas–liquid two-phase, increasing the mass transfer coefficient to 1–3 orders of magnitude to the traditional packed bed [32]. RPB is also widely used in the field of gas purification due to its small size of equipment, stable operation, convenient startup/shutdown, low energy consumption and low cost [33,34].

Based on this theory, we used a RPB as the absorption device and investigated its removal performance for NO using PS with activation of Fe^{2+}-EDTA. The main purpose of this article was to study the influence of operating parameters such as gas flow, gas–liquid ratio, high gravity factor, ammonium PS concentration, NO inlet concentration and O_2 exist on system performance. Identification of active species and products was carried out by ion chromatography and electron paramagnetic resonance spectrometer which revealed the NO removal pathway. The strengthening mechanism of RPB for NO removal was studied and the results also provided the theoretical guidance for the industrial applications of NO oxidation absorption.

2 Experimental

2.1 Experimental materials

NO (5%), O_2 (99%) and N_2 (99.9%) were used as the source of gas stream (they were purchased in Taineng Gas Co., Ltd.). $(NH_4)_2S_2O_8$ (99.0%), $FeSO_4 \cdot H_2O$ and disodium ethylenediaminetetraacetate were all of analytical reagents. All solutions were prepared using the deionized water.

2.2 Experimental setup

The experimental setup was mainly composed of a flue gas preparation system, a gas−liquid reaction system, a detection system and an exhaust gas treatment system as shown in Fig. 1 while the RPB was schematically shown in Fig. 2. The simulated flue gas in this experiment was composed of NO, N_2 and O_2 completely mixed in the buffer tank (5) and the concentration and flow rate were controlled by a gas flow meter which flowed from the buffer tank to the gas inlet (7.3) of the RPB (7) in the form of a continuous phase. Under the action of pressure, the flue gas entered the rotating packing layer from the bottom of the packing (7.2) along the axis, and passed through the packing layer after cross-flow contact with

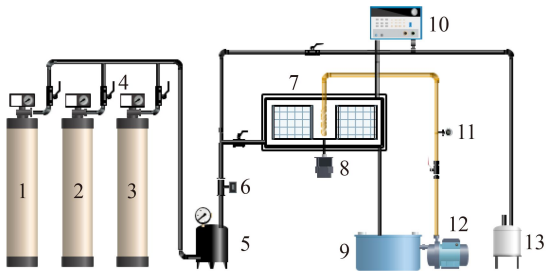

Fig. 1 Schematic diagram of experimental setup (1. Steel cylinder for NO; 2. Steel cylinder for N_2; 3. Steel cylinder for O_2; 4. Valve unit; 5. Gas buffer tank; 6. Gas flow meter; 7. Homemade RPB; 8. Motor; 9. Solution storage tank; 10. Flue gas analyzer; 11. Liquid flow meter; 12. Pump; 13. Tail gas absorber).

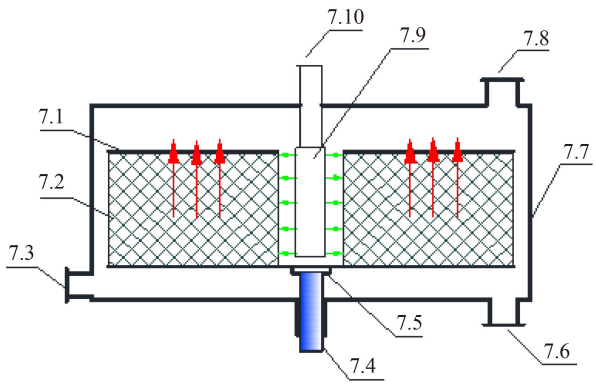

Fig. 2 Schematic diagram of RPB (7.1-rotor, 7.2-packing, 7.3-gas inlet, 7.4-shaft, 7.5-shaft seal, 7.6-liquid outlet, 7.7-cabinet, 7.8-gas outlet, 7.9-liquid distributor, 7.10-liquid inlet).

the absorbing liquid in the packing. The PS/Fe^{2+}-EDTA solution was introduced from solution storage tank (9) and was injected into the RPB by the liquid distributor (7.9). The liquid was evenly sprayed to the inner edge of the packing by the liquid distributor. Under the action of centrifugal force, it was spread and split into liquid elements like micro-scale droplets, thread or film, and moved along the inner edge of the packing to the outer edge. The high-speed liquid elements contacted cross-current with the flowing gas to activate the removal process of NO in flue gas, and then are discharged through the gas outlet (7.8) and liquid outlet (7.6), respectively. The inner and outer diameters of the rotor (7.1) was respectively 30 and 120 mm while the axial height was 70 mm. And the packing used in this study was a stainless steel wire mesh having a diameter of 0.25 mm and was wound around in the rotor with 95% porosity. The installed rotating packing was in a fixed cabinet (7.7) and was rotated at an adjustable speed. Data was recorded when the flue gas flowed through the flue gas analyzer (10) before and after the reaction. The exhaust gas could be further processed through the exhaust gas absorber (13).

2.3 Analytical method

The flue gas analyzer (KM9106) was used to determine the import and export concentrations of NO. Iron species (Fe^{2+} and Fe^{3+}) were determined spectrophotometrically using DRA-2500 spectrophotometer while the ion chromatography (ICS-1100) was used to determine the NH_4^+, SO_4^{2-}, NO_2^- and NO_3^- in solution. The electron paramagnetic resonance spectrometer (EPR, MS5000X) was used to detected the $\bullet SO_4^-$, •OH and $\bullet O_2^-$ by combining with 5,5-dimethyl-1-pyrroline N-oxide (DMPO) (> 99%) as a spin trapping agent to trap inorganic radicals. The pH meter (PHS-3C) monitored the initial and final pH values of each experiment adjusted by the addition of NaOH and HCl.

2.4 Data-processing method

The experimental results evaluated the NO removal effect of PS/Fe^{2+}-EDTA/RPB system by the change of NO concentration in the gas phase. The η_{NO} in the simulated flue gas can be calculated with the following formula:

$$\eta_{NO} = \frac{C_{NO,in} - C_{NO,out}}{C_{NO,in}} \times 100\%, \tag{1}$$

where $C_{NO,in}$ is the inlet concentration of NO in the simulated flue gas, ppm; $C_{NO,out}$ is the outlet concentration of NO in the simulated flue gas, ppm (10^{-6}); η_{NO} is the removal efficiency. The total volumetric mass transfer coefficient ($K_G\alpha$, s^{-1}) of RPB was calculated as follows [35]:

$$K_G\alpha = \frac{Q_G}{\pi h(r_2^2 - r_1^2)} NTU, \tag{2}$$

where Q_G is gas flow, $m^3 \cdot h^{-1}$; h is axial height of packing, m; r_1, r_2 are the inner and outer radius of the filler, respectively, m; NTU is the number of mass transfer units [36] and the calculation formula is as follows:

$$NTU = \int_{C_{out}}^{C_{in}} \frac{1}{C - C^*} \mathrm{d}C, \tag{3}$$

where C^* represents the equilibrium concentration of gas at the gas–liquid interface and the studies have shown that the absorption and oxidation process of NO in the PS system is a quasi-first-order rapid reaction [37], so C^* can usually be assumed to be 0. Therefore, the $K_G\alpha$ can be written as:

$$K_G\alpha = \frac{Q_G}{\pi h(r_2^2 - r_1^2)} \ln \frac{C_{in}}{C_{out}}. \tag{4}$$

3 Results and discussion

3.1 The influence of gas flow on η_{NO}

As shown in Fig. 3, it was obvious that the η_{NO} showed a steady decline with the increase in the flue gas flow. When the gas flow increased from 1 to 10 $m^3 \cdot h^{-1}$, the η_{NO}

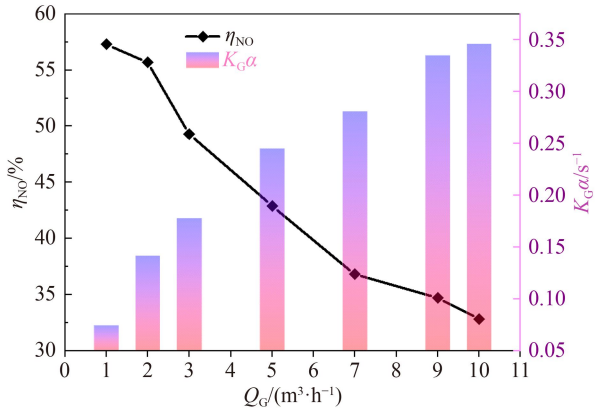

Fig. 3 The influence of gas flow on η_{NO} (conditions: C_A (NO concentration) = 500 ppm, C_B ($(NH_4)_2S_2O_8$ concentration) = 0.1 mol·L^{-1}, C (Fe^{2+}-EDTA) = 0.01 mol·L^{-1}, pH = 4.50, Q_L (liquid flow) = 60 L·h^{-1}, β (high gravity factor) = 68.21, T = 293 K).

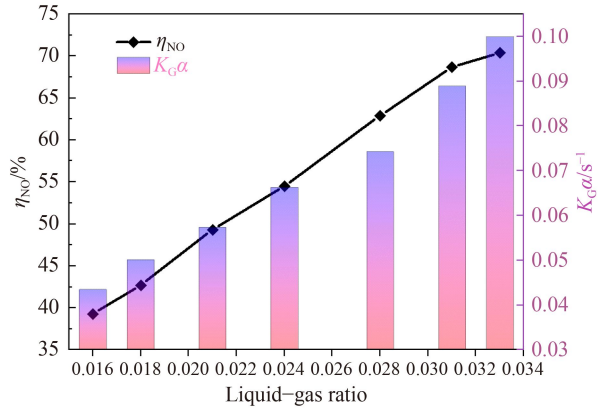

Fig. 4 The effect of liquid–gas ratio on η_{NO} (conditions: C_A = 500 ppm, C_B = 0.1 mol·L^{-1}, pH = 4.50, C (Fe^{2+}-EDTA) = 0.01 mol·L^{-1}, Q_G = 1 m^3·h^{-1}, β = 68.21, T = 293 K).

dropped from 57.3% to 32.8%. Increasing the gas flow would have increased the NO content, which reduced the molar ratio of oxidants to NO. At the same time, the speed of gas entering the packing was accelerated, which shortened the gas–liquid contact time, and the reaction could not be fully carried out. Only a part of NO reacted with the oxidizing substance, and most of the NO was blown out without participating in the reaction process, which was not conducive to NO removal. On the other hand, increasing the gas flow would have enhanced the turbulence of the gas phase which constantly updated the surface of liquid droplets and firms [38], and was beneficial to the mass transfer between gas and liquid. Thus the $K_G\alpha$ increased with the increase of gas flow. However, the effect of shortening the contact time and insufficient reaction was far greater than the effect of enhancement of mass transfer by increasing the gas flow, which reduced the removal efficiency of NO.

3.2 The effect of liquid–gas ratio on η_{NO}

Liquid–gas ratio is an important factor in absorption equipment, pumps, pipelines and investment, which directly affects the operation and cost of the system, and it is also considered as an effective method to adjust absorption performance. In this experiment, the influence of liquid–gas ratio on η_{NO} was investigated by changing the absorbent inlet flow.

As could be seen from Fig. 4, with the increase of liquid–gas ratio, η_{NO} and $K_G\alpha$ greatly increased. When liquid–gas ratio increased from 0.016 to 0.033, η_{NO} increased from 39.3% to 70.4%, and $K_G\alpha$ increased greatly from 0.0435 to 0.09996. When the gas flow was constant, the increasing of the liquid–gas ratio meant that the liquid flow increased. That made the circulation amount of PS, •SO_4^- and •OH through the reactor per unit time increase, which increased the relative molar ratio of oxidants to NO, hence the NO removal process was enhanced. On the other hand, the increase of the liquid volume not only increased the content of the oxidant, but also increased the wetting degree of the filler, the effective contact area of the gas–liquid and the turbulence of the liquid phase, thereby improving the mass transfer rate of NO in the gas–liquid phases and was beneficial for the removal process of NO. Therefore, under the condition that the gas flow remained unchanged, an appropriate increase in the liquid flow could effectively improve η_{NO} and $K_G\alpha$. However, the increase of the liquid flow would also have increased the energy consumption, so it was more appropriate to choose a gas–liquid value of about 0.033 in this experiment.

3.3 The influence of β on η_{NO}

According to the research methods of chemical engineering, dimensionless parameters are usually used to express the strength of the high gravity field, and that is the β, which is convenient for comparison of RPBs of different sizes and different speeds. It is defined as the ratio of centrifugal acceleration to gravitational acceleration at any place (or any point) in the high gravity field, and the Eq. (5) is [39]:

$$\beta = \frac{\omega^2 r}{g} = \frac{N^2 r}{900}, \tag{5}$$

where ω is the rotor angular speed, s^{-1}; r is the rotor radius, m; N is the rotor speed, r·min^{-1}, g is the gravitational acceleration, m·s^{-2}.

It can be seen from Eq. (5) that when the speed is constant, the β increases linearly with the rotor radius. Due to the different high gravity factors at different radius, the average β is generally used to describe the strength of the high gravity field as shown by Eq. (6):

$$\bar{\beta} = \frac{\int_{r_1}^{r_2} \beta \cdot 2\pi\, r\mathrm{d}r}{\int_{r_1}^{r_2} 2\pi\, r\mathrm{d}r} = \frac{2N^2(r_1^2 + r_1 r_2 + r_2^2)}{3 \times 900(r_1 + r_2)}. \tag{6}$$

Figure 5 shows the variation of $K_G\alpha$ and η_{NO} with β. The $K_G\alpha$ and η_{NO} obviously increased with an increase in β ranging from 4.85 to 77.61. When β exceeded 77.61, $K_G\alpha$ and η_{NO} still increased gradually, but the changes tended to be gentle, indicating that the positive effect of β on the η_{NO} began to decrease as well. When β increased, the speed of the filler would also increase, which would generate greater shear force, increase the cutting effect on the liquid, and accelerate the formation of smaller droplets and liquid film and the rate of surface renewal [31]. As a result, the mass transfer area of $\bullet SO_4^-$ and •OH–NO was increased, and the possibility of NO–$\bullet SO_4^-$(•OH) reaction on the liquid film surface was improved. When β was further increased, the liquid element further decreased, and the residence time of the element in the packing would have become shorter with the increase in the rotating speed, and the gas–liquid contact time decreased, which was not conducive to the chemical absorption process of NO and $S_2O_8^{2-}$, $\bullet SO_4^-$ and •OH. Hence the change of η_{NO} and $K_G\alpha$ tended to be flattened. The experimental results showed that the enhancement of mass transfer by increasing β was obviously higher than the adverse effect of residence time, but it also caused the increase of energy consumption. Thus, β of 77.61 was the best choice according to this study.

3.4 The influence of NO concentration on its removal efficiency

The influence of NO concentration on removal efficiency of NO was studied and the experimental results are shown in Fig. 6. With the increase of NO concentration, the η_{NO} and $K_G\alpha$ showed a downward trend. When NO concentration increased from 200 to 1000 ppm, the η_{NO} decreased from 75.1% to 65.1%, and the $K_G\alpha$ decreased from 0.1167 to 0.0971 s^{-1}. As the NO concentration increased, the gas-phase driving force became larger, which was conducive to gas-phase mass transfer. But increasing the NO concentration was equivalent to reducing the concentration of strong oxidizing groups per unit volume to remove NO, causing the slower liquid phase oxidation reaction rate and hindrance in the liquid phase mass transfer. The interaction caused the total mass transfer coefficient a gradual decrease, which further showed that the removal of NO by the advanced oxidation of $(NH_4)_2S_2O_8$ was a mass transfer control process.

3.5 The influence of $(NH_4)_2S_2O_8$ concentration on η_{NO}

PS concentration often has a large effect on free radical generation and pollutant removal and the influence of $(NH_4)_2S_2O_8$ concentration on η_{NO} was investigated, and the results are shown in Fig. 7. $K_G\alpha$ and η_{NO} increased with the increase of $(NH_4)_2S_2O_8$ concentration. The increase in the concentration of $(NH_4)_2S_2O_8$ meant that the content of $(NH_4)_2S_2O_8$ per unit liquid volume was increased, and the chances of contact with NO were also

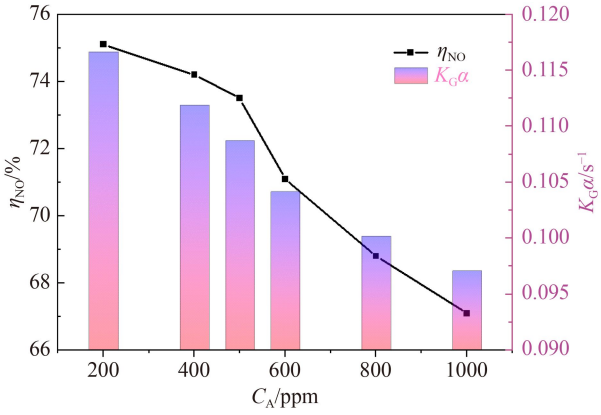

Fig. 6 Effect of NO inlet concentration on η_{NO} (conditions: C_B = 0.1 mol·L^{-1}, pH = 4.50, Q_G = 1 m^3·h^{-1}, L = 0.033, C (Fe^{2+}-EDTA) = 0.01 mol·L^{-1}, β = 77.61, T = 293 K).

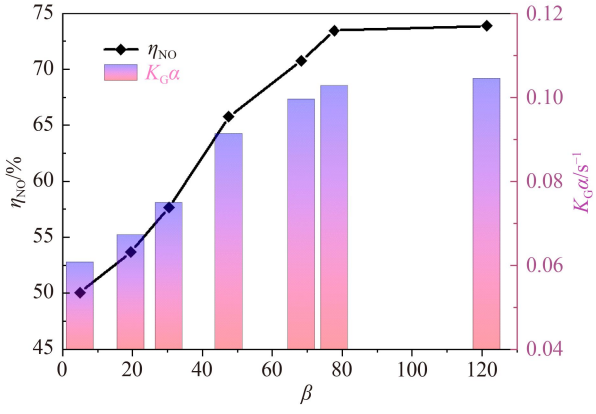

Fig. 5 The influence of β on η_{NO} (conditions: C_A = 500 ppm, C_B = 0.1 mol·L^{-1}, pH = 4.50, C (Fe^{2+}-EDTA) = 0.01 mol·L^{-1}, Q_G = 1 m^3·h^{-1}, L = 0.033, T = 293 K).

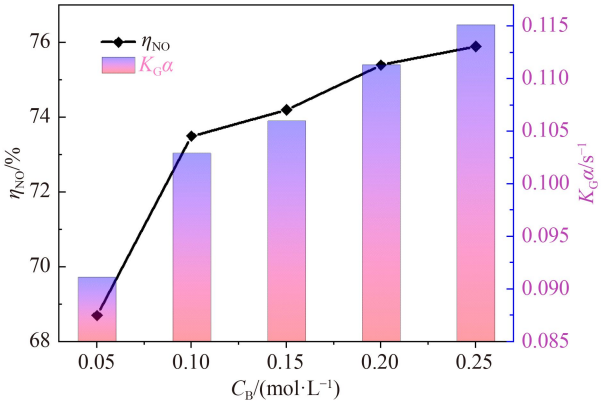

Fig. 7 Effect of $(NH_4)_2S_2O_8$ concentration on η_{NO} (conditions: C_A = 500 ppm, pH = 4.50, Q_G = 1 m^3·h^{-1}, β = 77.61, C (Fe^{2+}-EDTA) = 0.01 mol·L^{-1}, L = 0.033, T = 293 K).

increased, which effectively reduced the equilibrium partial pressure of the liquid solute and raised the driving force for mass transfer. Besides, Fe^{2+} effectively activated the PS to produce $\bullet SO_4^-$, which also could react with H_2O to produce •OH according to the Eqs. (7) and (8) [40]. As the C_B increased, the above (7) and (8) would accelerate and the yields of $\bullet SO_4^-$ and •OH would increase, thereby being able to enhance removal of NO (Eqs. (9)–(11)) [37]. When the concentration of $(NH_4)_2S_2O_8$ increased from 0.05 to 0.1 mol·L^{-1}, the change range of η_{NO} was 4.8% and when the concentration was increased from 0.1 to 0.25 mol·L^{-1}, the change range of η_{NO} was only 2.4%. This was because part of $\bullet SO_4^-$ were scavenged by Fe^{2+}, and high level $\bullet SO_4^-$ could also be consumed by itself and $S_2O_8^{2-}$ (Eqs. (12) and (14)) [41], causing a slight decrease in the increase of η_{NO}.

$$S_2O_8^{2-} + Fe^{2+} \xrightarrow{k_1=1.7-2.7 \text{ or } 2.0\times10 \text{ L·mol}^{-1}\text{·s}^{-1}(70°\text{C})} SO_4^{2-} + \cdot SO_4^- + Fe^{3+} \quad (7)$$

$$\cdot SO_4^- + H_2O \xrightarrow{k_2=6.6\times10^2 \text{s}^{-1}} HSO_4^- + OH\cdot \quad (8)$$

$$\cdot SO_4^- + NO + H_2O \xrightarrow{k_{sr}} HSO_4^- + NO_2^- + H^+ \quad (9)$$

$$\cdot OH + NO \xrightarrow{k_3=2\times10^{10} \text{L·mol}^{-1}\text{·s}^{-1}} H^+ + NO_2^- \quad (10)$$

$$NO_2^- + \cdot SO_4^- \xrightarrow{k_4=9.8\times10^8 \text{L·mol}^{-1}\text{·s}^{-1}} SO_4^{2-} + NO_2 \quad (11)$$

$$\cdot SO_4^- + Fe^{2+} \rightarrow SO_4^{2-} + Fe^{3+} \quad (12)$$

$$\cdot SO_4^- + \cdot SO_4^- \xrightarrow{k_5=4\times10^8 \text{L·mol}^{-1}\text{·s}^{-1}} S_2O_8^{2-} \quad (13)$$

$$\cdot SO_4^- + S_2O_8^{2-} \xrightarrow{k_6=6.1\times10^5 \text{L·mol}^{-1}\text{·s}^{-1}} SO_4^{2-} + \cdot S_2O_8^- \quad (14)$$

3.6 Mass transfer coefficient correlation formula calculation

The studies have shown that the mass transfer rate during the oxidation and absorption of NO by $\bullet SO_4^-$ and •OH were much smaller than the chemical reaction rate, and the process was controlled by mass transfer between gas and liquid [17,42]. Therefore, selecting the optimal conditions to achieve the best mass transfer coefficient was of great significance to NO oxidation and absorption. And in order to further clarify the relationship between the volumetric mass transfer coefficient and various factors, the correlation equation was solved by regression.

The relationship between the $K_G\alpha$ and influencing factors were as follows:

$$K_G\alpha = ZQ_G{}^x L^y \beta^z C_B^m C_A^n, \quad (15)$$

where Z is constant; L is the liquid–gas ratio, m^3·m^{-3}. After the logarithm of the two sides of the formula, the formula (16) was obtained:

$$\ln(K_G\alpha) = \ln Z + x\ln Q_G + y\ln L + z\ln\beta + m\ln C_B + n\ln C_A. \quad (16)$$

When the experimental data was sorted out and brought into the above formula, the parameters were calculated by regression as: Z = 0.397062; x = 0.6437; y = –0.50875; z = 0.19431; m = 0.14044; n = –0.11691.

The correlation formula of the total volume mass transfer coefficient can be expressed as:

$$K_G\alpha = \frac{0.397062\beta^{0.19431} C_B^{0.14044} Q_G{}^{0.6437}}{L^{0.50875} C_A^{0.11691}}. \quad (17)$$

The comparison of calculated value of $K_G\alpha$ and experimental value of $K_G\alpha$ in RPB is shown in Fig. 8. It was clearly shown that the calculated value was linearly related to the experimental value, and the slope of the straight line was 1.14, and the correlation coefficient R^2 was 0.99. The error of calculated value and experimental value were mostly within 15%. Accordingly, the $K_G\alpha$ could be well described by the formula (17) and it could found that the order of importance of different factors were gas flow, liquid–gas ratio, high gravity factor, ammonium persulfate concentration and NO concentration, providing guidance and optimization for the system.

3.7 The influence of O_2 on η_{NO}

The coal-fired flue gas contains certain amount of O_2, and its volume fraction is generally around 3% to 8%. Since Fe^{2+} is easily oxidized to Fe^{3+} by O_2 in the flue gas [43] and the Fe^{2+} concentration that can activate $(NH_4)_2S_2O_8$ decreases, which has a negative impact on the free radical yield. In the process of Fe^{2+}-EDTA activation of $(NH_4)_2S_2O_8$, O_2 competes with $(NH_4)_2S_2O_8$ to react with Fe^{2+}-EDTA, which affects the purification effect of NO. Figure 9 reflects the change of η_{NO} in the presence of O_2.

It could be seen from the Fig. 9 that when there was no oxygen in the simulated flue gas, the η_{NO} remained constant for a long time and the η_{NO} was higher when β

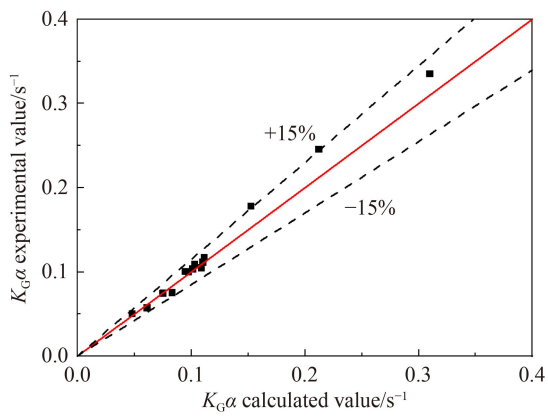

Fig. 8 Linear fit between experimental value and calculated value.

was 77.61 than that when β was 19.40. This was because when the β increased, the high-speed rotating packing generated more shear force. The absorbing liquid was spread and split into finer liquid micro-elements under the action of shear force, which significantly increased the gas–liquid contact area and strengthened the mass transfer. When O_2 existed (O_2 = 8%), the η_{NO} decreased, but the decreasing trend was different. Because O_2 in the flue gas continuously oxidized Fe^{2+}, producing inert Fe^{3+}-EDTA by reaction according to Eq. (18) [37,44], the partial deactivation of Fe^{2+} could not continue to participate in the activation process of $(NH_4)_2S_2O_8$, resulting in the decrease in η_{NO}. When β was 19.40, the variation of η_{NO} with time was larger than that when β was 77.61, and the η_{NO} declined more obviously and this phenomenon could be explained by the research results of Gambardella et al. [45]. When the mass transfer coefficient of the absorption equipment was larger, the absorption selectivity of NO could be improved. Besides, because the solubility of O_2 was smaller than that of NO, the oxidation reaction rate of O_2 and Fe^{2+}-EDTA was lower than that of NO and free radicals. When the β increased, the $K_G\alpha$ of the gas phase increased, which was beneficial to the removal of NO. Therefore, the decreasing trend of NO absorption efficiency was smaller when β was 77.61.

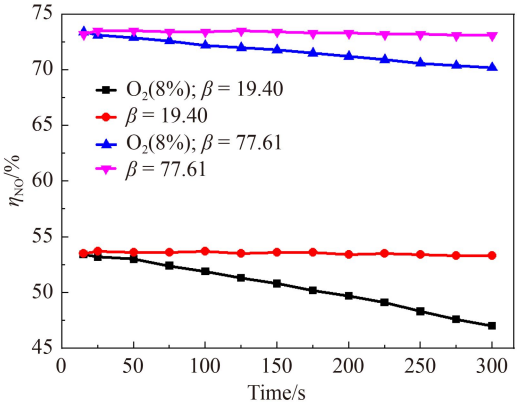

Fig. 9 The influence of O_2 on η_{NO} (conditions: C_A = 500 ppm, C_B = 0.1 mol·L^{-1}, pH = 4.50, Q_G = 1 m^3·h^{-1}, L = 0.033, C (Fe^{2+}-EDTA) = 0.01 mol·L^{-1}, β = 77.61, T = 293 K).

$$4Fe^{2+}\text{-EDTA} + O_2 + 2H_2O \rightarrow 4Fe^{3+}\text{-EDTA} + 4OH^- \quad (18)$$

In order to further clarify the changing trend of iron concentration in the process, the Fe^{2+} and Fe^{3+} in the solution were measured by UV spectrophotometry and the experimental results are shown in Fig. 10. It can be seen from Fig. 10 that when the oxygen concentration was 0%, Fe^{2+}-EDTA could keep the Fe^{2+} concentration in the liquid phase at about 0.004 mg·L^{-1} with the activator used to ensure the long-term and efficient activation of $(NH_4)_2S_2O_8$. The Fe^{3+} concentration was maintained at about 0.002–0.003 mg·L^{-1}, and it could be seen that large consumption of Fe^{2+} was not observed. When the oxygen concentration was 8%, the Fe^{2+} concentration was around 0.001 mg·L^{-1}, while the Fe^{3+} concentration showed a slight upward trend and the concentration was higher than that of when the oxygen concentration was 0%. The addition of oxygen caused part of the ferrous iron to react with it to form ferric iron, which was the main reason of reduced removal efficiency of NO.

3.8 Reaction pathways of NO removal

In order to further clarify the NO removal process in the reaction system, the components in the liquid phase and the gas phase were detected by an ion chromatograph and a flue gas analyzer as are arranged in Fig. S1 and Table 1.

A lot of ammonium ions were present in the solution, which were produced by the hydrolysis or ionization of $(NH_4)_2S_2O_8$ in the solution; and sulfate ions were mainly produced by the reaction of $\cdot SO_4^-$ and NO and the ineffective quenching of $\cdot SO_4^-$ (Eqs. (7)–(9), (19) [26]).

$$\cdot SO_4^- + \cdot OH \xrightarrow{k_7=1.0\times10^{10}\,\mathrm{L\cdot mol^{-1}\cdot s^{-1}}} HSO_4^- + \frac{1}{2}O_2 \quad (19)$$

At the same time, the material balance for S was carried out, and it was found that the sulfur content in the sulfate

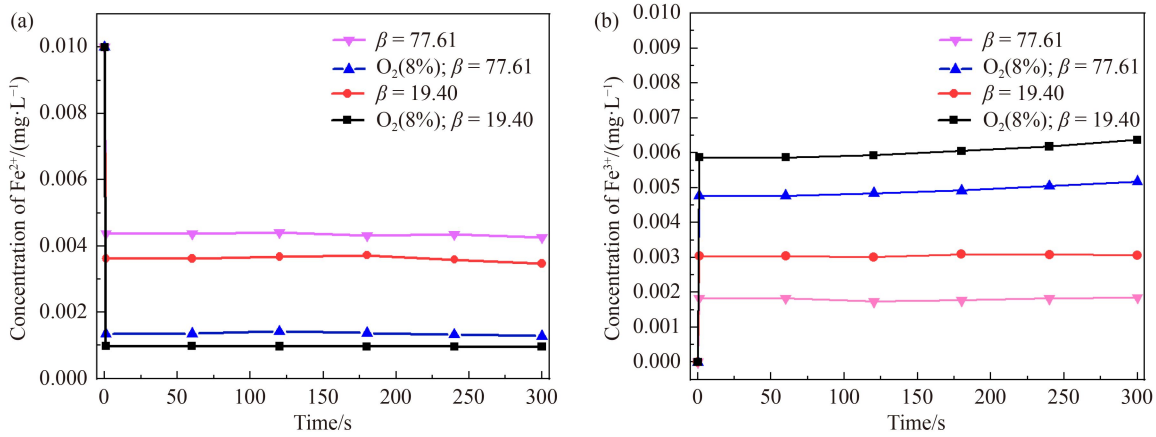

Fig. 10 Changes in the concentration of iron in the solution: (a) Concentration of Fe^{2+}, (b) Concentration of Fe^{3+}.

Table 1 Existence form of each substance after absorption[a)]

Time/s	Ion concentration/(mg·L^{-1})				
	NH_4^+	SO_4^{2-}	NO_3^-	NO_2^-	NO_2
150	3.32×10^3	0.432×10^2	9.16	–	–
300	3.41×10^3	0.871×10^2	18.22	–	–

a) Conditions: C_A = 500 ppm, C_B = 0.25 mol·L^{-1}, pH = 4.50, Q_G = 1 m^3·h^{-1}, β = 77.61, C (Fe^{2+}-EDTA) = 0.01 mol·L^{-1}, L = 0.033, T = 293 K.

ion was less than the total sulfur content, indicating that the solution contained unreacted PS ion. Nitrate ions were also detected in the reaction solution which were the products of NO oxidation. Based on the date in Table 1, a simple material balance had been performed and the calculation process and results are displayed in the ESM. As the reaction time increased, the concentration of sulfate ions and nitrate ions increased, indicating that the oxidation process was still going on, and PS could also directly oxidize NO (Eq. (20)) [46]. Meanwhile, nitrite ions and NO_2 were not detected in the reaction liquid and flue gas, because it eventually formed nitrate (Eqs. (21) and (22) [17]), indicating that the byproduct were not produced in the process.

$$S_2O_8^{2-} + NO + H_2O \rightarrow NO_2 + 2H^+ + 2SO_4^{2-} \quad (20)$$

$$2 \cdot SO_4^- + NO_2^- + H_2O \rightarrow NO_3^- + 2H^+ + 2SO_4^{2-} \quad (21)$$

$$NO_2 + \cdot OH \xrightarrow{k_8=4.5\times10^9 L\cdot mol^{-1}\cdot s^{-1}} H^+ + NO_3^- \quad (22)$$

To verify the existence of free radicals, EPR tests were performed. As shown in Fig. S2, •SO_4^- and •OH were successfully captured by electron spin resonance spectroscopy combining with DMPO. The seven-line peaks in the figure were the typical mixed spectrum shapes of •SO_4^- and •OH radical adducts, in which four circles represented •OH, and three rectangles represented •SO_4^-. Because of the peak overlap problem, the peak for •OH conformed approximately to the characteristic peak of •OH (1:2:2:1), and the characteristic peak of •SO_4^- as these were not obvious [21]. The measuring results demonstrated that both •SO_4^- and •OH were generated in the removal systems. Besides, as the reaction time was extended, •SO_4^- and • OH were still captured, reflecting that Fe^{2+}-EDTA could delay the release of free radicals. Meanwhile, a typical sextet EPR spectrum of superoxide free radicals (•O_2^-) was also monitored, which meant that activated PS could also generate •O_2^- (Eq. (23)) [47], which also indirectly acted on the oxidation process of NO.

$$2S_2O_8^{2-} + 2H_2O \rightarrow 3SO_4^{2-} + \cdot SO_4^- + \cdot O_2^- + 4H^+ \quad (23)$$

Based on the above experimental results and discussion, the mechanism of RPB/PS/Fe^{2+}-EDTA removal of NO system is summarized as follows: (1) •SO_4^- , •OH and •O_2^- were generated by Fe^{2+}-EDTA activated PS; (2) •SO_4^- and •OH could simultaneously oxidize NO to produce NO_3^-; (3) PS and •O_2^- could also oxidize NO to produce NO_3^-, but not playing a leading role; (4) Fe^{2+}-EDTA could delay the release of free radicals to improve free radical utilization; (5) the final products were NH_4NO_3 and $(NH_4)_2SO_4$; (6) the NO removal reaction had a better mass transfer process in the RPB/PS/Fe^{2+}-EDTA system. The above mechanism for NO removal may also be represented by the following Fig. S3.

4 Conclusions

The process and reaction mechanism of NO removal by PS oxidation in high gravity environment are studied and RPB was used as a gas–liquid absorption device to elevate the η_{NO} by aqueous $(NH_4)_2S_2O_8$ activated by Fe^{2+}-EDTA.

The results indicated that the η_{NO} increased with the increase of $(NH_4)_2S_2O_8$ concentration and liquid–gas ratio, but decreased with the increase of the gas flow. Increasing the high gravity factor from 4.85 to 77.61 was beneficial to the enhancement of η_{NO}. When the high gravity factor was higher than 77.61, the η_{NO} could reach 75% or higher. The η_{NO} was also found to decrease with a rise of NO concentration. And an empirical correlation could well predict the $K_G\alpha$ in this system. The order of importance of different factors were gas flow, liquid–gas ratio, high gravity factor, $(NH_4)_2S_2O_8$ concentration and NO concentration. In addition, the presence of O_2 in simulated flue gas had shown less effect on the NO removal process at higher speeds in RPB. Finally, according to the related references, determination of free radicals and analyses of removal products, the removal mechanism was speculated, in which, Fe^{2+}-EDTA could effectively activate $(NH_4)_2S_2O_8$ to produce the •SO_4^- and •OH, which were important for the oxidation from NO to NO_3^-, and the final products were NH_4NO_3 and $(NH_4)_2SO_4$, respectively. They are widely used in agricultural markets and are excellent nitrogen fertilizer. The NH_4NO_3 and $(NH_4)_2SO_4$ aqueous solutions are still further transformed into recoverable solids by crystallization and evaporation. Thus, it is foreseeable that RPB has great potential for industrial application in NO removal using persulfate as oxidant.

Acknowledgements The authors thank the National Natural Science Foundation of China International (Regional) Cooperation and Exchange Project (Grant No. 21961160740), the Shanxi Province Applied Basic Research Program (Grant No. 201901D111178) and 2021 Shanxi Postgraduate Innovation Project (Grant No. 2021Y601).

Electronic Supplementary Material Supplementary material is available in the online version of this article at https://dx.doi.org/10.1007/s11705-022-2224-5 and is accessible for authorized users.

References

1. Meng Z, Wang C, Wang X, Chen Y, Wu W, Li H. Simultaneous

removal of SO_2 and NO_x from flue gas using $(NH_4)_2S_2O_3$/steel slag slurry combined with ozone oxidation. Fuel, 2019, 255: 115760
2. Chen X, Hu X, Gao Y. Removal of NO in simulated flue with aqueous solution of peroxymonosulfate activated by high temperature and Fe(II). Chemical Engineering Journal, 2019, 359: 419–427
3. Adewuyi Y G, Khan M A. Nitric oxide removal from flue gas by combined persulfate and ferrous-EDTA solutions: effects of persulfate and EDTA concentrations, temperature, pH and SO_2. Chemical Engineering Journal, 2016, 304: 793–807
4. Hao R, Wang X, Mao X, Tian B, Zhao Y, Yuan B, Tao Z, Shen Y. An integrated dual-reactor system for simultaneous removal of SO_2 and NO: factors assessment, reaction mechanism and application prospect. Fuel, 2018, 220: 240–247
5. Hao R, Mao Y, Mao X, Wang Z, Gong Y, Zhang Z, Zhao Y. Cooperative removal of SO_2 and NO by using a method of UV-heat/H_2O_2 oxidation combined with NH_4OH-$(NH_4)_2SO_3$ dual-area absorption. Chemical Engineering Journal, 2019, 365: 282–290
6. Adewuyi Y G, Sakyi N Y, Arif Khan M. Simultaneous removal of NO and SO_2 from flue gas by combined heat and Fe^{2+} activated aqueous persulfate solutions. Chemosphere, 2018, 193: 1216–1225
7. Huang H, Hu H, Fan M, Chen J, Yuan S, Annanurov S. Mechanistic research on NO removal by $K_2S_2O_8$ with electrochemical catalysis. Chemical Engineering Journal, 2020, 382: 122873
8. Liu Y, Zhang J, Pan J, Tang A. Investigation on removal of NO from SO_2-containing simulated flue gas by UV/Fenton-like reaction. Energy & Fuels, 2012, 26(9): 5430–5436
9. Li G, Wang B, Xu W Q, Li Y, Han Y, Sun Q. Simultaneous removal of SO_2 and NO_x from flue gas by wet scrubbing using a urea solution. Environmental Technology, 2019, 40(20): 2620–2632
10. Wang L, Zhao W, Wu Z. Simultaneous absorption of NO and SO_2 by Fe^{II}-EDTA combined with Na_2SO_3 solution. Chemical Engineering Journal, 2007, 132(1–3): 227–232
11. Zhang Q, Wang S, Zhang G, Wang Z, Zhu P. Effects of slurry properties on simultaneous removal of SO_2 and NO by ammonia-Fe(II)EDTA absorption in sintering plants. Journal of Environmental Management, 2016, 183: 1072–1078
12. Zhao Y, Guo T, Chen Z, Du Y. Simultaneous removal of SO_2 and NO using M/$NaClO_2$ complex absorbent. Chemical Engineering Journal, 2010, 160(1): 42–47
13. Han Z, Yang S, Pan X, Zhao D, Yu J, Zhou Y, Xia P, Zheng D, Song Y, Yan Z. New experimental results of NO removal from simulated flue gas by wet scrubbing using NaClO solution. Energy & Fuels, 2017, 31(3): 3047–3054
14. Han Z, Gao Y, Yang S, Dong J, Pan X, Lan T, Song L, Yan Z, Sun D, Ning K N O. Removal from simulated diesel engine exhaust gas by cyclic scrubbing using $NaClO_2$ solution in a rotating packed bed reactor. Journal of Chemistry, 2019, 2019: 1–9
15. Chu H, Chien T W, Li S Y. Simultaneous absorption of SO_2 and NO from flue gas with $KMnO_4$/NaOH solutions. Science of the Total Environment, 2001, 275(1–3): 127–135
16. Shahrestani M M, Rahimi A, Momeni M. Experimental study and mathematical modeling of NO removal using the UV/H_2O_2 advanced oxidation process. Chemical Engineering & Technology, 2017, 40(6): 1149–1157
17. Liu Y, Wang Y. Simultaneous removal of NO and SO_2 using aqueous peroxymonosulfate with coactivation of Cu^{2+}/Fe^{3+} and high temperature. AIChE Journal, 2017, 63(4): 1287–1302
18. Wang Z, Wang Z, Ye Y, Chen N, Li H. Study on the removal of nitric oxide (NO) by dual oxidant (H_2O_2/$S_2O_8^{2-}$) system. Chemical Engineering Science, 2016, 145: 133–140
19. Adewuyi Y G, Sakyi N Y. Removal of nitric oxide by aqueous sodium persulfate simultaneously activated by temperature and Fe^{2+} in a lab-scale bubble reactor. Industrial & Engineering Chemistry Research, 2013, 52(41): 14687–14697
20. Adewuyi Y G, Sakyi N Y. Simultaneous absorption and oxidation of nitric oxide and sulfur dioxide by aqueous solutions of sodium persulfate activated by temperature. Industrial & Engineering Chemistry Research, 2013, 52(33): 11702–11711
21. Liu Y, Liu Z, Wang Y, Yin Y, Pan J, Zhang J, Wang Q. Simultaneous absorption of SO_2 and NO from flue gas using ultrasound/Fe^{2+}/heat coactivated persulfate system. Journal of Hazardous Materials, 2018, 342: 326–334
22. Zhen G, Lu X, Wang B, Zhao Y, Chai X, Niu D, Zhao A, Li Y, Song Y, Cao X. Synergetic pretreatment of waste activated sludge by Fe(II)-activated persulfate oxidation under mild temperature for enhanced dewaterability. Bioresource Technology, 2012, 124: 29–36
23. Adewuyi Y G, Khan M A, Sakyi N Y. Kinetics and modeling of the removal of nitric oxide by aqueous sodium persulfate simultaneously activated by temperature and Fe^{2+}. Industrial & Engineering Chemistry Research, 2014, 53(2): 828–839
24. Chen L, Ma J, Li X, Zhang J, Fang J, Guan Y, Xie P. Strong enhancement on fenton oxidation by addition of hydroxylamine to accelerate the ferric and ferrous iron cycles. Environmental Science & Technology, 2011, 45(9): 3925–3930
25. Liang C, Bruell C J, Marley M C, Sperry K L. Persulfate oxidation for *in situ* remediation of TCE. II. Activated by chelated ferrous ion. Chemosphere, 2004, 55(9): 1225–1233
26. Adewuyi Y G, Khan M A. Nitric oxide removal by combined persulfate and ferrous-EDTA reaction systems. Chemical Engineering Journal, 2015, 281: 575–587
27. Khan N E, Adewuyi Y G. Absorption and oxidation of nitric oxide (NO) by aqueous solutions of sodium persulfate in a bubble column reactor. Industrial & Engineering Chemistry Research, 2010, 49(18): 8749–8760
28. Gao X, Ma X, Kang X, Shi Y. Oxidative absorption of NO by sodium persulfate coupled with Fe^{2+}, Fe_3O_4, and H_2O_2. Environmental Progress & Sustainable Energy, 2015, 34(1): 117–124
29. Liu Y, Wang Y. Simultaneous removal of NO and SO_2 using aqueous peroxymonosulfate with coactivation of Cu^{2+}/Fe^{3+} and high temperature. AIChE Journal, 2017, 63(4): 1287–1302
30. Chen X, Hu X. Kinetics of the removal of NO using PMS-Fe(II) system activated by high temperature and Fe(II) ions in the multi-stage stirred bubble reactor. Chemical Engineering Journal, 2020,

379: 122144
31. Luo Y, Chu G, Zou H, Zhao Z, Dudukovic M P, Chen J. Gas−liquid effective interfacial area in a rotating packed bed. Industrial & Engineering Chemistry Research, 2012, 51(50): 16320–16325
32. Zhao H, Shao L, Chen J. High-gravity process intensification technology and application. Chemical Engineering Journal, 2010, 156(3): 588–593
33. Zhang L, Wang J, Sun Q, Zeng X, Chen J. Removal of nitric oxide in rotating packed bed by ferrous chelate solution. Chemical Engineering Journal, 2012, 181–182: 624–629
34. Guo J, Jiao W, Qi G, Yuan Z, Liu Y. Applications of high-gravity technologies in gas purifications: a review. Chinese Journal of Chemical Engineering, 2019, 27(6): 1361–1373
35. Sandilya P, Rao D P, Sharma A, Biswas G. Gas-phase mass transfer in a centrifugal contactor. Industrial & Engineering Chemistry Research, 2001, 40(1): 384–392
36. Adewuyi Y G, He X, Shaw H, Lolertpihop W. Simultaneous absorption and oxidation of NO and SO_2 by aqueous solutions of sodium chlorite. Chemical Engineering Communications, 1999, 174(1): 21–51
37. Liu Y, Wang Y, Xu W, Yang W, Pan Z, Wang Q. Simultaneous absorption−oxidation of nitric oxide and sulfur dioxide using ammonium persulfate synergistically activated by UV-light and heat. Chemical Engineering Research & Design, 2018, 130: 321–333
38. Li Y, Liu Y, Zhang L, Su Q, Jin G. Absorption of NO_x into nitric acid solution in rotating packed bed. Chinese Journal of Chemical Engineering, 2010, 18(2): 244–248
39. Jiao W, Liu Y, Qi G. A new impinging stream-rotating packed bed reactor for improvement of micromixing iodide and iodate. Chemical Engineering Journal, 2010, 157(1): 168–173
40. Romero A, Santos A, Vicente F, González C. Diuron abatement using activated persulphate: effect of pH, Fe(II) and oxidant dosage. Chemical Engineering Journal, 2010, 162(1): 257–265
41. Wang Q, Shao Y, Gao N, Chu W, Deng J, Shen X, Lu X, Zhu Y, Wei X. Degradation of alachlor with zero-valent iron activating persulfate oxidation. Journal of the Taiwan Institute of Chemical Engineers, 2016, 63: 379–385
42. Chen X, Hu X. Removal of NO_x and SO_2 from the coal-fired flue gas using a rotating packed bed pilot reactor with peroxymonosulfate activated by Fe(II) and heating. Energy & Fuels, 2019, 33(7): 6707–6716
43. Adewuyi Y G, Khan M A. Simultaneous NO and SO_2 removal by aqueous persulfate activated by combined heat and Fe^{2+}: experimental and kinetic mass transfer model studies. Environmental Science and Pollution Research International, 2020, 27(2): 1186–1201
44. Liu N, Lu B, Zhang S, Jiang J, Cai L, Li W, He Y. Evaluation of nitric oxide removal from simulated flue gas by Fe(II)EDTA/Fe(II)citrate mixed absorbents. Energy & Fuels, 2012, 26(8): 4910–4916
45. Gambardella F, Winkelman J G M, Heeres H J. Experimental and modelling studies on the simultaneous absorption of NO and in aqueous iron chelate solutions. Chemical Engineering Science, 2006, 61(21): 6880–6891
46. Hao R, Yang S, Yuan B, Zhao Y. Simultaneous desulfurization and denitrification through an integrative process utilizing $NaClO_2/Na_2S_2O_8$. Fuel Processing Technology, 2017, 159: 145–152
47. Furman O S, Teel A L, Watts R J. Mechanism of base activation of persulfate. Environmental Science & Technology, 2010, 44(16): 6423–6428